J Biomol NMR (2007) 38:243–253
DOI 10.1007/s10858-007-9165-7

ARTICLE

Refinement of protein structure against non-redundant carbonyl ^{13}C NMR relaxation

Nico Tjandra · Motoshi Suzuki · Shou-Lin Chang

Received: 24 January 2007 / Accepted: 11 May 2007 / Published online: 7 June 2007

Abstract Carbonyl $^{13}C'$ relaxation is dominated by the contribution from the $^{13}C'$ chemical shift anisotropy (CSA). The relaxation rates provide useful and non-redundant structural information in addition to dynamic parameters. It is straightforward to acquire, and offers complimentary structural information to the ^{15}N relaxation data. Furthermore, the non-axial nature of the $^{13}C'$ CSA tensor results in a T_1/T_2 value that depends on an additional angular variable even when the diffusion tensor of the protein molecule is axially symmetric. This dependence on an extra degree of freedom provides new geometrical information that is not available from the NH dipolar relaxation. A protocol that incorporates such structural restraints into NMR structure calculation was developed within the program Xplor-NIH. Its application was illustrated with the yeast Fis1 NMR structure. Refinement against the $^{13}C'$ T_1/T_2 improved the overall quality of the structure, as evaluated by cross-validation against the residual dipolar coupling as well as the ^{15}N relaxation data. In addition, possible variations of the CSA tensor were addressed.

Keywords Protein structure refinement · NMR · ^{15}N relaxation · $^{13}C'$ relaxation · Xplor-NIH · Yeast Fis1 protein

Electronic Supplementary Material The online version of this article (doi:10.1007/s10858-007-9165-7) contains supplementary material, which is available to authorized users.

N. Tjandra (✉) · M. Suzuki
Laboratory of Molecular Biophysics, National Heart, Lung, and Blood Institute, National Institutes of Health, Building 50, Room 3503, Bethesda, MD 20892, USA
e-mail: nico@helix.nih.gov

S.-L. Chang (✉)
Institute of Bioinformatics and Structural Biology, Department of Life Science, National Tsing Hua University, Life Science Building II, Room 338, 101, Sec. 2 Kuang Fu Rd, HsinChu 30055, Taiwan
e-mail: slchang@life.nthu.edu.tw

Introduction

Long-range information is crucial for accurate structure determination of biomolecules using NMR. This type of information is not available in the typical nuclear Overhauser enhancement (NOE) data that provide distance restraints limited to less than 5 Å, or scalar (J) coupling constants for nuclei separated by a few bonds. A wide range of methods are now available to gain this important information, such as paramagnetic enhancement (Bertini et al. 2001 2004; Biekofsky et al. 1999; Donaldson et al. 2001; Dvoretsky et al. 2002; Ikegami et al. 2004; Pintacuda et al. 2004; Prudêncio et al. 2004; Wöhnert et al. 2003) and dissolving biomolecules in dilute liquid crystalline media (Tjandra and Bax 1997; Tolman et al. 1995). Most of these techniques, however, involve changing the condition of the sample either by replacing its medium or inclusion of compounds that bind paramagnetic elements. One attractive alternative is to utilize the non-spherical shape of the biomolecules. The main advantage of this approach is that the shape is inherent in the molecule and no change of the sample condition is required. The shape of the molecule governs the way it diffuses in solution. In NMR, the rotational diffusion is best measured through relaxation times that has the dependence both on the rate of diffusion as well as the orientation of the spin interaction vector with respect to the external magnetic field, and therefore, the dependence on the geometry of the molecule (Woessner 1962). A non-spherical molecule diffuses asymmetrically resulting in a dependence of the relaxation

rates on the relative orientation of spin interaction vectors in the molecule.

This approach was initially illustrated using ^{15}N relaxation data to refine a 259-residue protein (Tjandra et al, 1997). Since then, there have been numerous applications of this method to the refinement of relative domain orientations in protein (Bruschweiler et al. 1995; Fushman et al. 1999). The structural information arises from the relative orientation of the relaxation interaction tensor with respect to the diffusion frame. In the case of ^{15}N relaxation, which is dominated by the dipolar interaction of ^{15}N nuclear spin with its directly bonded ^{1}H, the relaxation rates depend on how the NH bond is oriented with respect to the diffusion axis (Tjandra et al. 1995; Woessner 1962). The information obtained from ^{15}N relaxation is essentially the same as that in the NH residual dipolar coupling (RDC). Therefore, their potential applications and challenges are similar. Proteins with large anisotropy in their shape are particularly suitable for such an approach. Higher magnetic fields and increased sensitivity of modern spectrometers make the application of this method even more practical.

The dependence of ^{15}N relaxation on the NH bond orientation alone helps in defining long-range order in the system, as shown previously (Tjandra et al. 1997). Further improvement can be made by inclusion of other relaxation information that depends on different interaction vectors or tensors. Theoretically, any interactions that lead to relaxation can be measured and used as structural restraints. The degree of difficulty in the application of these restraints depends on how much these interactions can be isolated from one another. For the relaxation term that involves predominantly CSA contribution such as ^{13}C′ carbonyl, in general one has to assume that the CSA tensor is fully asymmetric (Cornilescu and Bax 2000; Oas et al. 1987; Pang and Zuiderweg 2000; Teng et al. 1992). This makes the general expression for the relaxation rates quite complicated. In addition, variations in the magnitude and direction of ^{13}C′ CSA tensor may further obstruct the interpretation of the relaxation rates.

At the outset, it is important to emphasize that this approach is not designed to replace or compete with dipolar coupling refinement. Most dipolar couplings will have a larger range, thus will be more practical for structure refinement. The implementation of relaxation data in structure refinement will inherently contain some approximations due to the complicated relaxation pathways or mechanisms and dynamic influences. On the other hand, similar problems are also encountered in the interpretation of NOE as well as cross-correlated relaxation data. Nevertheless, the main goal in developing this method is to provide an alternative in cases where no suitable alignment media can be found. This approach will also offer an additional means to independently validate a structure.

Here we describe the development of a protocol using ^{13}C′ carbonyl relaxation to improve the quality of a protein structure in a straightforward manner. We show that the structural information contained in the ^{13}C′ relaxation is not redundant with the ^{15}N relaxation data. A consistent refinement protocol against the two datasets is also established. Application of this protocol to the refinement of the protein yeast Fis1 (Suzuki et al 2005) improved both the precision and accuracy, as measured by the rmsd (root-mean-square-deviation) and RDC cross-validation of the calculated structures, respectively.

Materials and methods

Sample preparation

The ^{15}N-labeled and ^{15}N-, ^{13}C-labeled yeast Fis1 protein was expressed and purified as described previously (Suzuki et al. 2005). Samples for NMR relaxation experiments contained 1.0 mM protein in 10 mM Tris acetate buffer at pH 5.5, with 5% D_2O.

Measurements of the ^{15}N longitudinal relaxation time T_1 and transverse relaxation time T_2

NMR ^{15}N relaxation experiments were performed at 32°C on a Bruker DRX 600-MHz spectrometer for the ^{15}N-labeled yeast Fis1 sample. The temperature was calibrated by measuring the chemical shift difference between the proton signal of 3-(Trimethylsilyl)-1-propanesulfonic acid sodium salt (TSP) and the proton signal of water. The spectrometer was equipped with a shielded x,y,z-pulsed field gradient unit and a triple-resonance 5-mm probe. States-TPPI quadrature detection in the t_1 dimension was used for all experiments. The ^{15}N and ^{1}H carrier frequencies were set to 116.5 ppm and the water frequency, respectively. NMR data were processed using NMRPipe (Delaglio et al. 1995) and analyzed with PIPP software (Garrett et al. 1991). The pulse sequences, acquisition parameters and data analysis procedures employed were as previously described (Tjandra et al. 1997). The T_1 and $T_{1\rho}$ delays were optimized for the yeast Fis1 protein. They were 12, 52, 204, 404, 644, 884, 1024, 1604 ms and 6.9, 14.1, 16.1, 38.1, 57.3, 76.5, 100.5, 124.5 ms for T_1 and $T_{1\rho}$, respectively. The $T_{1\rho}$ values were converted to T_2 values by taking into account the T_1 relaxation time, the chemical shift offset from the carrier, and the spin-lock field strength as described in Tjandra et al. (1997).

Measurement of the ^{13}C-carbonyl carbon relaxation times T_1 and T_2

Carbonyl carbon relaxation experiments were performed at 32 °C on a Bruker DRX 600-MHz spectrometer for the

^{13}C- and ^{15}N-labeled yeast Fis1 sample. The temperature for each measurement was calibrated as described in ^{15}N relaxation experiments. Similar pulse sequences as in Chang and Tjandra (2005) were used with variations in the T_1 relaxation delays (8, 150, 300, 500, 800, 1100, 1500, 2400 ms) as well as the $T_{1\rho}$ delays (4, 15, 30, 45, 60, 75, 95, 120 ms). The same data analysis was used to extract the relaxation rates and their corresponding experimental errors. The $T_{1\rho}$ values were converted to the T_2 values in a similar fashion as described for the ^{15}N measurements.

Expressions for relaxation rates

The general equations for longitudinal (R_1) and transverse relaxation (R_2) rates for spin-1/2 nuclei can be divided into CSA and dipolar (DD) contributions (Spiess 1978). They are given below:

$$R_1^{CSA} = \frac{1}{T_1^{CSA}} = \gamma_I^2 B_o^2 \left[g_2^{CS}(\omega)\right] \quad (1)$$

$$R_2^{CSA} = \frac{1}{T_2^{CSA}} = \frac{1}{2}\gamma_I^2 B_o^2 \left[g_2^{CS}(\omega) + \frac{3}{4} g_2^{CS}(0)\right] \quad (2)$$

$$R_1^{DD} = \frac{1}{T_1^{DD}} = \gamma_I^2 \gamma_s^2 \hbar^2 \left[\frac{1}{3} g_2^D(\omega_I - \omega_S) + g_2^D(\omega_I) + 2g_2^D(\omega_I + \omega_s)\right] \quad (3)$$

$$R_2^{DD} = \frac{1}{T_2^{DD}} = \frac{1}{2}\gamma_I^2 \gamma_S^2 \hbar^2 \left[\frac{4}{3} g_2^D(0) + \frac{1}{3} g_2^D(\omega_I - \omega_s) + g_2^D(\omega_I) + 2g_2^D(\omega_S) + 2g_2^D(\omega_I + \omega_S)\right] \quad (4)$$

where $\hbar$ is the Planck's constant over 2π and γ is the gyromagnetic ratio. The indices *CSA* and *DD* represent the contributions from CSA and dipolar interaction, respectively. In the case of ^{13}C′ relaxation, the index *I* represents the ^{13}C′ and the index *S* represents all the nuclear spins that are involved in the dipolar interaction with it, such as $^{13}C_\alpha$, amide ^{15}N, H_α, and amide H_N, which are included in our calculation, plus other distant carbons, nitrogens and protons. The function $g(\omega)$ has been described previously (Spiess 1978; also see the table provided in the Electronic Supplementary Material). It contains the dynamic contributions such as the overall diffusion and internal motion as well as the geometrical factors describing the relationship between the interaction frame and the diffusion frame. Expressions for the $g(\omega)$ were derived for an asymmetric interaction tensor experiencing an asymmetric overall rotational diffusion. In the case of ^{15}N relaxation, the ^{15}N-^{1}H dipolar interaction vector and ^{15}N CSA tensor are approximately axially symmetric and parallel with each other. Therefore, the equations reduce to those described in Tjandra et. al. (1996).

The situation for ^{13}C′ relaxation is not as simple due to the asymmetric nature of the ^{13}C′ CSA tensor. Therefore, the full treatment needs to be considered. The Euler angles α, β, and γ in the $g(\omega)$ function describe the relative orientation of the interaction tensor to the diffusion frame. These angles as well as the CSA tensor for ^{13}C′ in the local molecular frame are illustrated in Fig. 1. At lower magnetic fields the dipolar contributions to the ^{13}C′ relaxation rates are not negligible with the largest fraction coming from the dipolar interaction between the ^{13}C′ and the surrounding protons. The relaxation rates depend on the distance between these atoms. In an anisotropic molecule, relaxation will also depend on the relative orientation of the dipole to the diffusion tensor. It is not trivial to properly account for this contribution without a prior knowledge of the protein structure. Fortunately, our simulations showed that inclusion of the C′-H_N and C′-H_α dipolar contributions to the ^{13}C′ relaxation accounts for a large fraction of the dipolar terms from protons in the relaxation rates. Using this approach to analyze the ^{13}C′ relaxation data acquired at the 400-, 600- and 800-MHz spectrometer results in a maximum of 4%, 3% and 2% error in T_1/T_2 ratio, respectively, for a protein with a correlation time of 10 ns. This is expected since an increase in the magnetic field strength will make the contribution from CSA more dominant.

Protein size has a complicated effect on the approximation we made in the dipolar terms with two different factors contributing. One is the correlation time and the other is the proton density. At small correlation times, the proton density is important. At larger correlation times or larger proteins, the increasing number of protons does not lead to increasing error in the approximation since the dipolar terms drop off significantly as inter-nuclear distance increases above 6 Å. Our simulation estimated a maximum error of about 2% as a function of correlation time up to 15 ns at 600 MHz spectrometer frequency.

Estimate of the overall diffusion tensor

A good estimate of the overall effective correlation time, $(2D_{zz} + 2D_{yy} + 2D_{xx})^{-1}$, diffusion anisotropy, $2D_{zz}/(D_{xx} + D_{yy})$, and rhombicity, $3/2\ (D_{yy} - D_{xx})/[D_{zz} - 0.5(D_{yy} + D_{xx})]$, is important in obtaining a reasonably fast convergence of the calculated structures to their global minimum. Typically, one can fit the T_1/T_2 ratios to a known structure to obtain an accurate estimate of the diffusion tensor. In a situation where a high-precision structure is not available, as in our case, an acceptable estimate

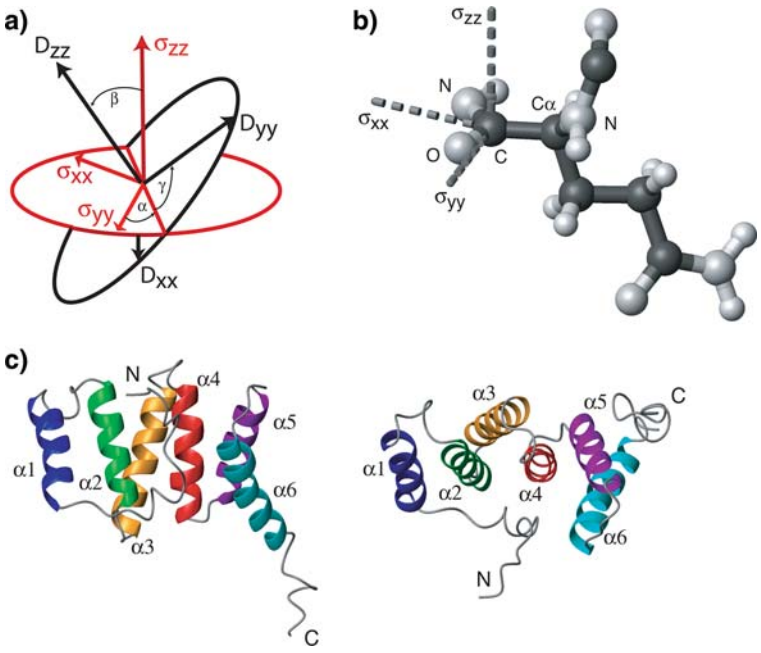

Fig. 1 (**a**) The relationship between the $^{13}C'$ chemical shift anisotropy tensor and the overall rotational diffusion tensor is defined by the three Euler angles α, β, and γ. (**b**) The local CSA tensor is defined within the peptide plane of Q40 of yeast Fis1, with the three tensor components σ_{xx}, σ_{yy}, and σ_{zz}. (**c**) A ribbon representation of yeast Fis1 protein. These are two different views to illustrate the asymmetry in the shape of the molecule. Figure 1b and c were created by the program MOLMOL (Koradi et al. 1996)

can be derived from the distribution of T_1/T_2 values (Clore et al. 1998). This estimate can then be optimized using a multi-dimensional grid search method during the structure calculation itself. The best diffusion tensor is determined by the one that gives the lowest overall energy of the calculated structure.

Structure calculation

The ^{13}C carbonyl refinement was implemented as a module in Xplor-NIH (Schwieters et al. 2003). The complete relaxation treatments as described in Eqs. 1–4 were included in the refinement module. During the calculation, the relaxation times are evaluated as a function of the local tensor frame (CSA and dipolar) relative to the diffusion frame. In representing the diffusion tensor coordinate system, four pseudo atoms (OO, XX, YY, and ZZ) are chosen. The three vectors connecting the atom OO to the other atoms define the diffusion axis. Incorporation and handling of this axis system during the calculation is the same as in the residual dipolar coupling refinement. Note that this is quite different from the original implementation for the ^{15}N relaxation refinement (Tjandra et al. 1997), where the T_1/T_2 value was approximated as a $\cos(\theta)$ expansion, where θ is the angle between the NH bond and the unique axis of the diffusion tensor. This was done because the NH relaxation interaction tensors as well as the diffusion tensor were assumed to be axially symmetric. This is clearly not the case for the ^{13}C carbonyl relaxation, thus the need for the complete expressions for relaxation to be employed. To avoid the dependence of structure refinement on the local fast order parameter (S^2) and the corresponding internal correlation time (τ_e), an empirical energy function that depends only on the difference between measured and calculated T_1/T_2 value is also used (Kay et al. 1989) as shown below:

$$E_{diffusion} = k\left[\left(\frac{T_1}{T_2}\right)_{calc} - \left(\frac{T_1}{T_2}\right)_{meas}\right]^2 \tag{5}$$

where k is a force constant. The value for k is adjusted during the calculation to a final value that results in the overall rmsd between the measured and calculated T_1/T_2 being equal to the estimated experimental errors. An alternative to this is to use the squared well potential given below:

$$\begin{aligned} E_{diffusion} &= 0, && \text{for} \quad \left|\left(\frac{T_1}{T_2}\right)_{calc} - \left(\frac{T_1}{T_2}\right)_{meas}\right| \geq \Delta_{\min} \\ & && \text{and} \quad \left|\left(\frac{T_1}{T_2}\right)_{calc} - \left(\frac{T_1}{T_2}\right)_{meas}\right| \leq \Delta_{\max} \\ E_{diffusion} &= k\left[\left(\frac{T_1}{T_2}\right)_{calc} - \left(\frac{T_1}{T_2}\right)_{meas}\right]^2 && \text{for} \quad \left|\left(\frac{T_1}{T_2}\right)_{calc} - \left(\frac{T_1}{T_2}\right)_{meas}\right| < \Delta_{\min} \\ & && \text{or} \quad \left|\left(\frac{T_1}{T_2}\right)_{calc} - \left(\frac{T_1}{T_2}\right)_{meas}\right| > \Delta_{\max} \end{aligned} \tag{6}$$

where Δ_{min} and Δ_{max} are the lower and upper bounds of the T_1/T_2 value that can be estimated from the experimental errors.

Results

The relaxation-based structure refinement was applied to the yeast Fis1 protein. The original structure of this protein was determined using the typical NOE, dihedral, and residual dipolar couplings restraints (Suzuki et al. 2005). The Fis1, an all α-helical protein as depicted in Fig. 1c, is expected to tumble asymmetrically as suggested from its molecular shape. A total of 113 and 77 sets of T_1 and T_2 value were obtained for the backbone ^{15}N and $^{13}C'$, respectively, for the yeast Fis1. The T_1/T_2 ratios for ^{15}N and $^{13}C'$ as a function of residue number are shown in Fig. 2. Several residues must be excluded from the analysis due to their large-amplitude fast motion or slow conformational exchange. Fast internal motion with substantial amplitude will affect the T_1 but not the T_2 values, while the exchange contribution will only affect the T_2 values. These will result in either underestimate or overestimate of the T_1/T_2. A very conservative steady-state ^{15}N-^{1}H NOE cutoff of 0.75 was used to exclude the residues K3-T9, G33, G34, E71-E73, H106-N110, and Q125-H144 due to fast internal motion. Additionally, residue I85 can be identified to undergo slow conformational exchange by a statistical test (Barbato et al. 1992). Any residues identified using the above criteria in either the ^{15}N or $^{13}C'$ datasets were excluded from the refinement. In addition, residues with spectral overlap were also excluded. A final 68 ^{15}N and 63 $^{13}C'$ T_1/T_2 values were used in the refinement. Their distributions are shown in Fig. 2c, d. The histograms for both ^{15}N and $^{13}C'$ are consistent and they clearly suggest fully asymmetric diffusion (Clore et al. 1998) as expected from the yeast Fis1 structure. The ^{15}N T_1/T_2 distribution is not as well represented as the $^{13}C'$ data. This is due to the dominant N-H dipolar interaction in the ^{15}N T_1/T_2 in a fully helical protein that will not isotropically sample all of the possible orientations. The asymmetric $^{13}C'$ CSA, however, is expected to produce a better geometrical sampling. The estimated experimental errors were 1.17 and 2.74% for ^{15}N and $^{13}C'$ T_1/T_2, respectively. These errors were obtained by comparing two independent T_1 or T_2 datasets acquired under similar conditions but at different times. The errors for the T_1/T_2 values were then propagated from the T_1 and T_2 errors.

It is useful to simulate the T_1/T_2 values for ^{15}N and $^{13}C'$ in order to evaluate their different sensitivity in a structure refinement. Figure 3 shows the dependence of T_1/T_2 on the angle β at various values of anisotropy and rhombicity. The angle β is defined as in Fig. 1 for $^{13}C'$ relaxation, while for ^{15}N case it is formed between the NH dipolar interaction vector and the unique axis of the diffusion tensor. It is clear from Fig. 2 that the $^{13}C'$ T_1/T_2

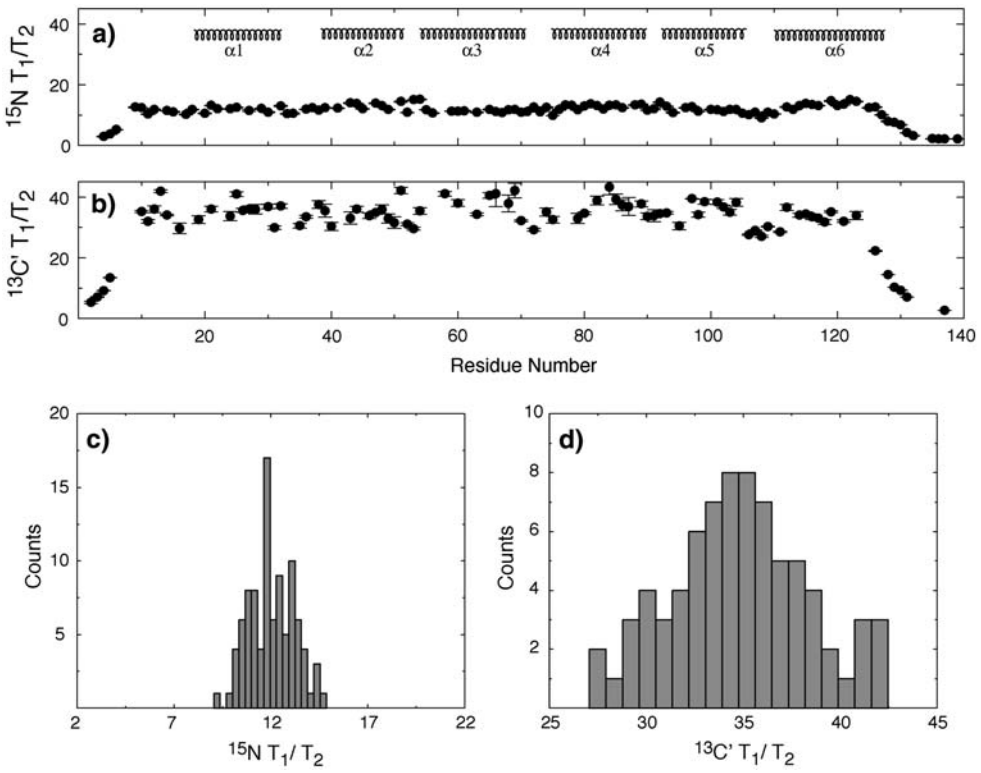

Fig. 2 The ^{15}N (**a**) and $^{13}C'$ (**b**) T_1/T_2 values are plotted as a function of the residue number of yeast Fis1. The distribution of the T_1/T_2 values for ^{15}N and $^{13}C'$ are shown as histograms in (**c**), and (**d**) panels, respectively. The histograms only reflect residues that are actually used in the structure refinement. They exclude residues that undergo large amplitude fast motions or slow conformational exchange

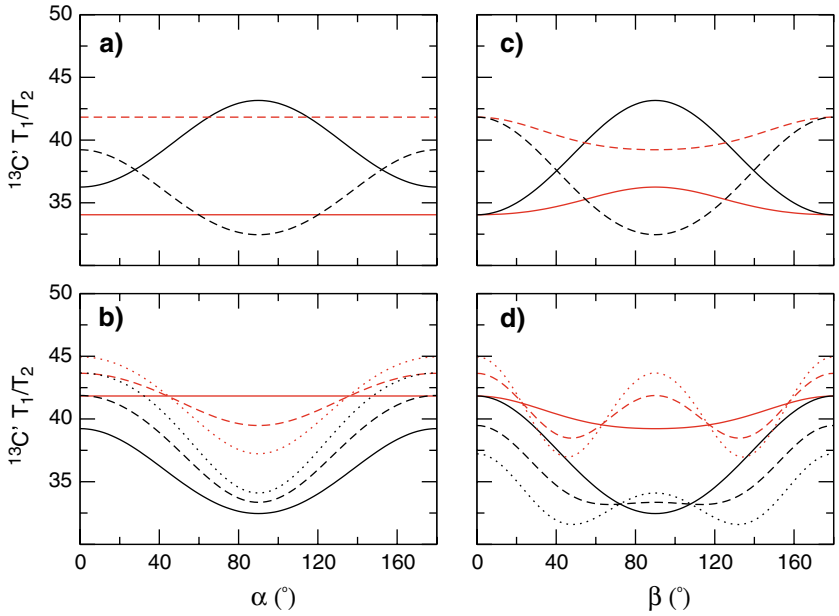

Fig. 3 Simulated values of $^{13}C'$ T_1/T_2 are plotted as a function of the angle α and calculated for various diffusion parameters. (**a**) The $^{13}C'$ T_1/T_2 values are calculated for anisotropy of 0.7 (solid lines) or 1.4 (dashed lines) and angle β of 0 (red) or 90° (black). (**b**) These values are also calculated for different rhombicity: 0 (solid lines), 0.5 (dashed lines), and 1.0 (dotted lines). Similar calculations are plotted as a function of the angle β for various anisotropy (**c**) and rhombicity (**d**), with values identical to those used in calculating a & b. The α angle of 0°, and 90° is designated with red and black, respectively. In all of these calculations the rhombicity is fixed to 0 when varying anisotropy, and anisotropy is fixed to 1.4 while varying rhombicity

values have almost twice the range as the ^{15}N T_1/T_2 values, and their averages also differ by a factor of two. Thus, for refinement purposes, $^{13}C'$ relaxation results in comparable sensitivity in differentiating small β angles in the structure as in the case of ^{15}N T_1/T_2. The distribution of the $^{13}C'$ T_1/T_2 data is different from the ^{15}N values when the rhombicity is zero. This is due to the non-axially symmetric $^{13}C'$ CSA tensor. Even when the diffusion tensor is fully asymmetric, the ^{15}N T_1/T_2 has no dependence on the angle α, while the $^{13}C'$ T_1/T_2 always has strong dependence on this angle (Fig. 3). The dependence of relaxation on one extra degree of freedom ensures that the information contained in the $^{13}C'$ T_1/T_2 data is not redundant compared to the ^{15}N T_1/T_2. In addition, these nuclear relaxations are sensitive to distinct local structural variations. This is illustrated by the correlation between the two datasets plotted in Fig. 4. The correlation plot was made for $^{13}C'$ and ^{15}N data on the same peptide plane and the label follows the residue number of the ^{15}N. The correlation coefficient R for the two datasets is –0.49. The negative correlation slope is a result of the relative orientation of the NH dipolar vector that is perpendicular to the σ_{zz} axis of the $^{13}C'$ CSA tensor (Cornilescu and Bax 2000). The experimental errors are much smaller than the scatter in the correlation indicating that there is different structural information contained in the $^{13}C'$ and ^{15}N T_1/T_2. This is quite similar to the comparison between residual dipolar coupling which is axial in nature versus residual CSA that is non-axial (Lipsitz and Tjandra 2003). The same argument applies here, a rotation of the local structure around the NH bond will leave the ^{15}N T_1/T_2 invariant, while the same rotation will change the $^{13}C'$ T_1/T_2. Therefore it is definitely advantageous to include the $^{13}C'$ T_1/T_2 in the refinement to improve the overall quality of the calculated structure. It is also important to point out that any large dynamic influence on only one of the dataset will affect the correlation plot. For instance, I85 of yeast Fis1 undergoes conformational exchange. Its real $^{13}C'$ T_2 value is underestimated, thus resulting in an overestimate of the T_1/T_2. Interestingly the ^{15}N relaxations do not indicate any possible exchange contribution and the T_1/T_2 value still falls within the expected distribution. However, in the T_1/T_2 correlation plot I85 is clearly above the correlation distribution suggesting that the $^{13}C'$ frequency is better at probing the conformational exchange rate of I85 than that of ^{15}N. Residues with large-amplitude fast internal motion will in general have low T_1 values resulting in an underestimate of the T_1/T_2. For example residues E107-N110 are in the flexible part of the molecule, have underestimated ^{15}N and $^{13}C'$ T_1/T_2 values, and fall well below the correlation distribution. Only these residues are shown in Fig. 4 for clarity, but this observation is true for all residues identified with large-amplitude fast internal motion.

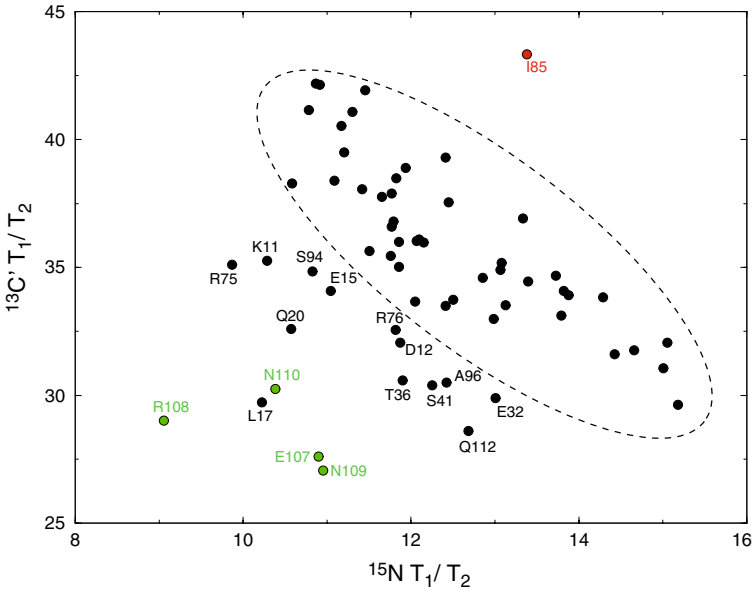

Fig. 4 A correlation plot of ^{15}N T_1/T_2 vs. $^{13}C'$ T_1/T_2, with a calculated correlation coefficient of –0.49 for all residues in black. The correlation is for ^{15}N and $^{13}C'$ data on the same peptide plane. The label follows the residue number of ^{15}N data. The Residue marked in red (I85) is above the correlation region due to conformational exchange. Residues in green have T_1 values that are too low due to fast internal motion

The $^{13}C'$ T_1/T_2 refinement was carried out on yeast Fis1 with the original structural restraints as reported in Suzuki et al. (2005) except that the dipolar coupling restraints were intentionally left out and reserved to be used as a cross validation. A total of 100 structures were calculated, from which the 10 lowest energy structures were chosen to represent the ensemble. A harmonic restraint was used for all of the ^{15}N and $^{13}C'$ T_1/T_2 values with a targeted final rmsd equal to their respective experimental errors. To achieve this, the force constant k was slowly increased from an initial value of 0.0001 kcal/mol to a final value of 1 kcal/mol. An initial estimate for the diffusion parameters was obtained by the distribution method using ^{15}N data. The initial values used in the refinement of ^{15}N were 10.6 ns, 1.3, and 0.8 for the overall correlation time, anisotropy, and rhombicity, respectively. These values were later optimized by the grid search method to be 10.7 ns, 1.5, and 0.5 for ^{15}N relaxation data. As previously observed, a slight difference in sample condition can lead to changes in τ_c (Chang and Tjandra 2005). The yeast Fis1 ^{15}N and $^{13}C'$ datasets were acquired using different samples, therefore a separate grid search optimization was needed for the $^{13}C'$ data. An optimized τ_c of 9.8 ns was found for the $^{13}C'$ relaxation data. The changes in the total energy as functions of the optimized variables are plotted in Fig. 5. The overall minimum can clearly be observed in addition to some local minima. As expected, the energy surface is not very smooth. This is especially true when the starting structure is not very well refined, as in the case of yeast Fis1. Therefore the grid search approach was more preferable than an automatic gradient minimization to overcome the local minima. Moving away from the global minimum results in worse accuracy and worse precision in

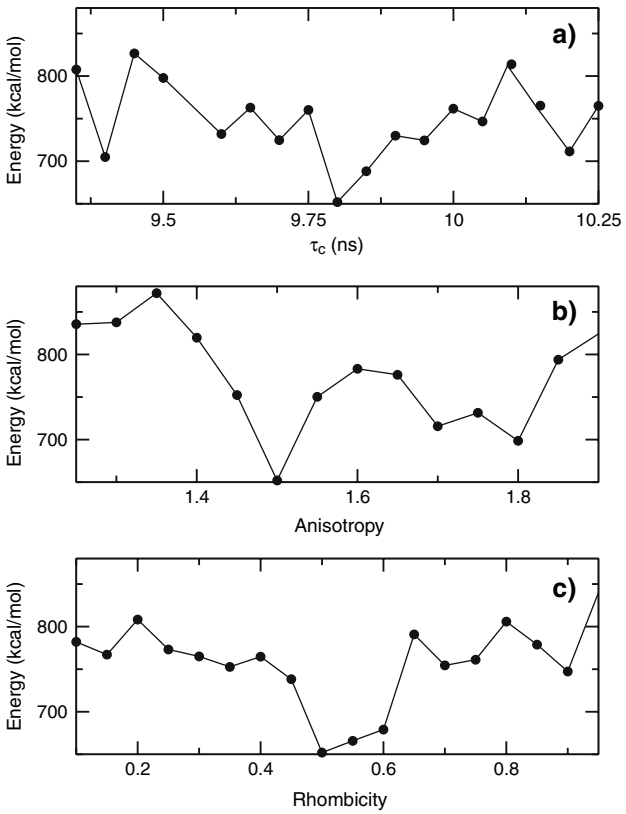

Fig. 5 The total energy is plotted as functions of (**a**) overall correlation time (τ_c), (**b**) anisotropy, and (**c**) rhombicity

the refined structures. For structures refined with both ^{15}N and $^{13}C'$ relaxation restraints (''All T_1/T_2'' in Tables 1 and 2), moving to the second minimum on τ_c, anisotropy and rhombicity will lead to an increase in backbone and RDC rmsd up to 0.62 Å and 5.07 Hz, respectively, and a drop in

Table 1 Comparison of the best 10 structures refined with and without relaxation data

Restraints	rmsd to RDC (Hz)[b]	rmsd to ^{15}N T_1/T_2	rmsd to ^{13}C′ T_1/T_2	Backbone rmsd (Å)[a]
NOE[c]	5.19 ± 0.44	0.69 ± 0.08	2.68 ± 0.16	0.65
^{15}N T_1/T_2	3.97 ± 0.42	0.24 ± 0.03	2.65 ± 0.53	0.58
^{13}C′ T_1/T_2	5.15 ± 0.52	0.59 ± 0.07	1.45 ± 0.14	0.57
All T_1/T_2	4.71 ± 0.58	0.31 ± 0.02	1.42 ± 0.08	0.55

[a] The structures were least-square fit using the backbone atoms of residues L10-I124

[b] The calculated structures were best fit to the NH RDC

[c] These structures were calculated based on the published original data sets excluding the RDC. Final force constants used in the structure refinements are 5 and 1 kcal/mol for ^{15}N and ^{13}C′ T_1/T_2, respectively

Table 2 Residue statistics in the Ramachandran plot of the best 10 structures refined with and without relaxation data

Restraints	Most favored region (%)	Additional allowed region (%)	Generously allowed region (%)	Disallowed region (%)
NOE	74.2	22.7	1.6	1.6
^{15}N T_1/T_2	80.5	15.6	2.3	1.6
^{13}C′ T_1/T_2	75.0	18.8	6.3	0.0
All T_1/T_2	78.1	14.8	5.5	1.6

the percentage of the ''most favorable region'' in the Ramachandran plot to 74%.

The Fis1 protein structures refined with and without relaxation restraints were compared by evaluating the difference in the measured and calculated T_1/T_2 values. The result of the refinement is summarized in Table 1. The refinement protocol improved the agreement between the calculated T_1/T_2 and their experimental values. However, other independent indicators are needed to evaluate the resulting precision and accuracy of the structure. Clearly, the precision of the structures improved as measured by the decrease in the rmsd value from 0.6 to 0.5 Å when relaxation data was included in the refinement. It is not surprising that with each addition of a new restraint dataset that is consistent with the existing ones, the precision of the structures increases. This alone, however, is not a complete measure of the structure accuracy. A good way to assess this is to use cross-validation as measured by agreement to other independent data (Cornilescu et al. 1998; Ottiger and Bax 1999). In our case, the agreement of the relaxation-refined structures to the residual dipolar couplings available for the yeast Fis1 can be estimated. In addition one can also use the ^{15}N T_1/T_2 values to estimate structure quality (de Alba and Tjandra 2000). This is done by leaving the ^{15}N T_1/T_2 values out of the structure refinement and then see how the resulting structures refined with ^{13}C′ T_1/T_2 agree with the ^{15}N T_1/T_2 values. The rmsd of the ten best structures to the NH RDC is 5.15± 0.52 Hz, while the rmsd to the ^{15}N T_1/T_2 is 0.59 ± 0.07 (Table 1). This results in marginal improvement compared to the structures refined without ^{13}C′ T_1/T_2 and can be attributed to the extra degree of freedom that the ^{13}C′ T_1/T_2 is sensitive to. For example, changes that lead to effective rotation of the peptide plane around the NH bond will not affect the ^{15}N T_1/T_2 or the NH RDC, but they will modulate the ^{13}C′ T_1/T_2. A similar observation was made for ^{15}N $\Delta\delta$ (chemical shift anisotropy) evaluation. Only a small improvement in ^{15}N $\Delta\delta$ agreement could be obtained when a structure is refined with NH RDC (Lipsitz and Tjandra 2003). Even though this was a site-specific comparison between the ^{15}N $\Delta\delta$ and NH RDC, an additional degree of freedom can make the two datasets quite distinct. Therefore, evaluation based on the NH bond geometry (NH RDC and ^{15}N T_1/T_2) on ^{13}C′ T_1/T_2 refined structure is not optimal. However, if one looks at the results when ^{15}N T_1/T_2 is used in addition to the ^{13}C′ T_1/T_2, the convergence (based on ^{13}C′ T_1/T_2 rmsd) and the RDC agreement improve. These data indicate that the information contained in the relaxation and the residual dipolar coupling data are consistent and their inclusion in the structure calculation results in the improvement of precision and accuracy of the structure. The percentage of the ''most favorable region'' in the Ramachandran plot increases for the structures refined with relaxation restraints as shown in the Table 2.

Discussion

There is a practical advantage in being able to obtain long-range information in high resolution NMR without changing the sample condition. Theoretically, the ^{13}C′ relaxation contains long-range information. Since it is dominated by ^{13}C′ CSA, the T_1/T_2 resulting from the asymmetric ^{13}C′ CSA tensor will depend on an additional

degree of freedom compared to the ^{15}N data. This provides extra geometrical dependence. Furthermore the weak correlation between the ^{13}C′ T_1/T_2 and the ^{15}N T_1/T_2 establishes two objectives. First, it proves that the two datasets are consistent, since both should depend on the local geometry, namely the orientation of the peptide plane. Second, this weak correlation also illustrates the additional degree of freedom that the ^{13}C′ T_1/T_2 contains.

In order to use the ^{13}C′ T_1/T_2 data for refinement efficiently, a good estimate for the overall diffusion parameters is required. Conceptually one can fit the starting structure to the ^{13}C′ T_1/T_2 and obtain the overall diffusion parameters. For an average NMR structure, this fit would typically be poor. One can still use these parameters weakly in the ^{13}C′ T_1/T_2 refinement as a first approximation. It can then be iterated to improve the estimate and the refined structure. This can only be accomplished when there are additional structural data such as NOE and dihedral information that are consistent and relatively noise free. An alternative approach was suggested previously (Clore et al. 1998), where the distribution of ^{15}N T_1/T_2 values is used for the estimate. It is similar to the one applied to the residual dipolar couplings for the estimate of alignment tensor components. This would bring the overall diffusion parameters closer to the real values but does not alleviate the necessity for iteration by grid search for further optimization. With a limited number of T_1/T_2 values, all possible orientations of the relaxation interaction tensor will not be sampled, thus resulting in a non-representative distribution. In the case of yeast Fis1 a relatively good estimate of the overall diffusion parameters can be obtained by the second approach. The initial estimate for τ_c, anisotropy, and rhombicity is within 1, 15, and 41%, respectively, from their optimal values. This is acceptable given the sparse number of data points.

The inclusion of ^{13}C′ T_1/T_2 in the refinement protocol increased the quality of the calculated structures. The assessment of this improvement needs to be carried out carefully, since any addition of structural data is always expected to improve the precision of the structures. Provided that the ^{13}C′ T_1/T_2 is not redundant, a check of its consistency with other available datasets for the yeast Fis1 structure is an independent measure of the quality of its information content. This was done by cross-validation of the ^{13}C′ T_1/T_2 with the NH RDCs and ^{15}N T_1/T_2 datasets. The rmsd of 5.15 Hz and 0.59 for NH RDCs and ^{15}N T_1/T_2, respectively, shows that indeed the structures refined with the ^{13}C′ T_1/T_2 restraints are consistent with other datasets. It is difficult at this time to provide a limit for an acceptable rmsd value for the ^{13}C′ T_1/T_2, since so far there is only one example. However, one can expect to obtain similar numbers as in the case of ^{15}N T_1/T_2 (de Alba and Tjandra 2000).

The residue-specific variation of the ^{13}C′ CSA tensor needs to be taken into consideration. The magnitude of this variation is still under intensive study. The work of Cornilescu and Bax (Cornilescu and Bax 2000) provides an estimate for the variations in the ^{13}C′ CSA tensor. They found an upper limit of 10 ppm in the variation based on the differences between measured residual ^{13}C′ CSA and the expected values estimated from the X-ray structure of ubiquitin. They also suggested a possible variation in the tensor direction by 17°. This was pointed out to be an overestimate due to the sampling of the data points as well as the contribution from structural noise. In our case, we are interested in how much the calculated structure will change as a function of the variation of the ^{13}C′ CSA. The variation in both magnitude and direction of the CSA tensor will affect the outcome of the calculated structure. The residue-specific variation is small. In fact the possible error raised due to this variation will be within our experimental error. Nevertheless, this does put an upper limit on how well one can refine the structure even in the presence of noiseless data.

Changes in the average ^{13}C′ CSA used will also influence the refined structure. In fact this evaluation has been carried out previously in the application of residual ^{13}C′ CSA refinement (Lipsitz and Tjandra 2001). No large changes in the structures could be observed when the ^{13}C′ CSA tensor was varied within the range of published values. The reason for this insensitivity was due to the broad energy minimum. Since the way relaxation depends on the ^{13}C′ CSA tensor is different from the way the residual CSA depends on the ^{13}C′ CSA tensor, it is not clear if the same conclusion can be drawn. Therefore, a series of structure refinements were carried out with varying CSA tensor magnitudes to see how they affect the calculated structures. The resulting structures differ at most by an rmsd of 0.8 Å when σ_{zz} is changed by 20%, while a similar change in the asymmetry η of the CSA tensor results in an rmsd of 1.1 Å. These are relatively large changes in the CSA tensor magnitudes that lead to structural changes. Under real physical CSA variation, the structural deviation can be expected to be within the error of the calculated structures.

In addition to possible variations in the ^{13}C′ CSA, assumptions made for the order parameters (S^2) need to be considered as well. As pointed out earlier (Chang and Tjandra, 2005), the order parameter is not easily defined for ^{13}C′ relaxation. Fluctuating fields caused by the ^{13}C′ CSA, ^{13}C′–^{1}H, ^{13}C′–^{13}C, and ^{13}C′–^{15}N dipolar interactions all contribute to the ^{13}C′ relaxation. In principle, the motion associated with these interactions is anisotropic and uncorrelated. A different order parameter is required to describe the motional amplitude of each interaction tensor or vector. It is practically impossible to carry out such an analysis, considering the large number of variables and

limited relaxation rates available from the experiments. In order to simplify the process, an effective order parameter must be used in this case. Of course the site-specific variation in the order parameter rather than their absolute magnitudes is more relevant to the structure refinement. If one adheres to the cutoff criteria used to eliminate the data points that might contain large-amplitude fast internal motion or slow conformational exchange, this variation will be reduced. In addition, the utilization of the T_1/T_2 ratio as a structural restraint further minimizes the dependence of the empirical energy function on the order parameter.

Another source of error is the approximated contribution to the $^{13}C'$ relaxation rates from the dipolar interaction between the $^{13}C'$ and its neighboring protons (Chang and Tjandra 2005). In the structure refinement, only the $C'–H^N$ and $C'–H^{\alpha}$ dipolar contributions were taken into account. This is expected, based on our simulation, to account for a large fraction of the dipolar terms. Since the density of protons around each of the $^{13}C'$ is not the same, one would expect that some error will be introduced by this approximation. However more importantly, the variation in the rate depends also on the direction of these dipoles in an anisotropically diffusing molecule. Therefore, to be able to estimate these dipolar contributions properly, a prior knowledge of the structure is required. We in fact calculate the $C'–H^N$ and $C'–H^{\alpha}$ contributions in a completely anisotropic treatment for each refinement step. It is also possible to calculate all dipolar contributions for all protons around each $^{13}C'$ site. This unfortunately will not be very computationally practical other than for very small proteins. In addition to the C′–H dipoles, one also must consider at least $C'–C_{\alpha}$ as well as C′–N dipolar contributions. These contributions are also fully taken into account for each refinement step.

Carbonyl ^{13}C relaxations are relatively uncomplicated to measure (Allard and Härd 1997; Chang and Tjandra 2005; Dayie and Wagner 1995, 1997; Engelke and Rüterjans, 1997; Ishima et al.2004; Mulder and Akke 2003). We showed that the $^{13}C'$ T_1/T_2 data offer long-range information that is non-redundant compared to the ^{15}N relaxation-based structural information. The availability of the data to be measured without changing the sample condition is one of its attractive features. The potential use of the $^{13}C'$ relaxation for refinement depends on the diffusion anisotropy of the molecule. We have minimized the number of assumptions that go into the calculation of the $^{13}C'$ relaxation rates. This ensures the general applicability and robustness of the refinement protocol without paying a large penalty in the computational time. Potentially, other relaxation-based refinements can be developed using the same approach presented here.

Acknowledgments Part of this work was supported by the Intramural Research Program of the NIH, National Heart, Lung, and Blood Institute to N.T.

References

Allard P, Härd T (1997) NMR relaxation mechanisms for backbone carbonyl carbons in a ^{13}C, ^{15}N-labeled protein. J Magn Reson 126:48–57

Barbato G, Ikura M, Kay LE, Pastor RW, Bax A (1992) Backbone dynamics of Calmodulin studied by ^{15}N relaxation using inverse detected 2-dimensional NMR spectroscopy – The central helix is flexible. Biochemistry 31:5269–5278

Bertini V, Janik MBL, Lee Y-M, Luchinat C, Rosato R (2001) Magnetic susceptibility tensor anisotropies for a lanthanide ion series in a fixed protein matrix. J Am Chem Soc 123:4181–4188

Bertini I, Bianco CD, Gelis I, Katsaros N, Luchinat C, Parigi G, Peana M, Provenzani A, Zoroddu MA (2004) Experimentally exploring the conformational space sampled by domain reorientation in calmodulin. Proc Natl Acad Sci 101:6841–6846

Biekofsky RR, Muskett FW, Schmidt JM, Martin SR, Browne JP, Bayley PM, Feeney J (1999) NMR approaches for monitoring domain orientations in calcium-binding proteins in solution using partial replacement of Ca^{2+} by Tb^{3+}. FEBS Lett 460:519–526

Bruschweiler R, Liao X, Wright PE (1995) Long-range motional restrictions in a multidomain zinc-finger protein from anisotropic tumbling. Science 268:886–889

Chang S-L, Tjandra N (2005) Temperature dependence of protein backbone motion from carbonyl ^{13}C and amide ^{15}N NMR relaxation. J Magn Reson 174:45–53

Clore GM, Gronenborn AM, Szabo A, Tjandra N (1998) Determining the magnitude of the fully asymmetric diffusion tensor from heteronuclear relaxation data in the absence of structural information. J Am Chem Soc 120:4889–4890

Cornilescu G, Marquardt JL, Ottiger M, Bax A (1998) Validation of protein structure from anisotropic carbonyl chemical shifts in a dilute liquid crystalline phase. J Am Chem Soc 120:6836–6837

Cornilescu G, Bax A (2000) Measurement of proton, nitrogen, and carbonyl chemical shielding anisotropies in a protein dissolved in a dilute liquid crystalline phase. J Am Chem Soc 122:10143–10154

Dayie KT, Wagner G (1995) Carbonyl-carbon relaxation rates reveal a dynamic heterogeneity of the polypeptide backbone in villin 14T. J Magn Reson Series B 109:105–108

Dayie KT, Wagner G (1997) Carbonyl carbon probe of local mobility in ^{13}C, ^{15}N-enriched proteins using high-resolution nuclear magnetic resonance. J Am Chem Soc 119:7797–7806

de Alba E, Tjandra N (2000) Protein backbone ^{15}N relaxation rates as a tool for the diagnosis of structure quality. J Magn Reson 144:367–371

Delaglio F, Grzesiek S, Vuister GW, Zhu G, Pfeifer J, Bax A (1995) NMRPipe: a multidimensional spectral processing system based on UNIX pipes. J Biomol NMR 6(3):277–93

Donaldson LW, Skrynnikov NR, Choy W-Y, Muhandiram DR, Sarkar B, Forman-Kay JD, Kay LE (2001) Structural characterization of proteins with an attached ATCUN motif by paramagnetic relaxation enhancement NMR spectroscopy. J Am Chem Soc 123:9843–9847

Dvoretsky A, Gaponenko V, Rosevear PR (2002) Derivation of structural restraints using a thiol-reactive chelator. FEBS Lett 528:189–192

Engelke J, Rüterjans H (1997) Backbone dynamics of proteins derived from carbonyl carbon relaxation times at 500, 600, and

800 MHz: application to ribonuclease T1. J Biomol NMR 9:63–78

Fushman D, Xu R, Cowburn D (1999) Direct determination of changes of interdomain orientation on ligation: Use of the orientational dependence of ^{15}N NMR relaxation in Abl SH(32). Biochemistry 38(32):10225–10230

Garrett DS, Powers R, Gronenborn AM, Clore GM (1991) A common-sense approach to peak picking in 2-dimensional, 3-dimensional, and 4-dimensional spectra using automatic computer analysis of contour diagrams. J Magn Reson 95:214–220

Ikegami T, Verdier L, Sakhaii P, Grimme S, Pescatore B, Saxena K, Fiebig KM, Griesinger C (2004) Novel techniques for weak alignment of proteins in solution using chemical tags coordinating lanthanide ions. J Biomol NMR 29(3):339–349

Ishima R, Baber J, Louis JM, Torchia DA (2004) Carbonyl carbon transverse relaxation dispersion measurements and ms-μs timescale motion in a protein hydrogen bond network. J Biomol NMR 29:187–198

Kay LE, Torchia DA, Bax A (1989) Backbone dynamics of proteins as studied by ^{15}N inverse detected heteronuclear NMR spectroscopy: application to staphylococcal nuclease. Biochemistry 28(23):8972–8979

Koradi R, Billeter M, Wuthrich K (1996) MOLMOL: a program for display and analysis of macromolecular structures. J Mol Graph 14:51–55

Lipsitz RS, Tjandra N (2001) Carbonyl CSA restraints from solution NMR for protein structure refinement. J Am Chem Soc 123(44):11065–11066

Lipsitz RS, Tjandra N (2003) ^{15}N Chemical shift anisotropy in protein structure refinement and comparison with NH residual dipolar couplings. J Magn Reson 164:171–176

Mulder FAA, Akke M (2003) Carbonyl ^{13}C transverse relaxation measurements to sample protein backbone dynamics. Magn Reson Chem 41:853–865

Oas TG, Hartzell CJ, McMahon TJ, Drobny GP, Dahlquist FW (1987) The carbonyl ^{13}C chemical shift tensors of five peptides determined from ^{15}N dipole-coupled chemical shift powder patterns. J Am Chem Soc 109:5956–5962

Ottiger M, Bax A (1999) Bicelle-based liquid crystals for NMR measurement of dipolar couplings at acidic and basic pH values. J Biomol NMR 13:187–191

Pang Y, Zuiderweg ER (2000) Determination of protein backbone ^{13}CO chemical shift anisotropy tensors in solution. J Am Chem Soc 122:4841–4842

Pintacuda G, Moshref A, Leonchiks A, Sharipo A, Otting G (2004) Site-specific labelling with a metal chelator for protein-structure Refinement. J Biomol NMR 29(3):351–361

Prudêncio M, Rohovec J, Peters JA, Tocheva E, Boulanger MJ, Murphy MEP, Hupkes H-J, Kosters W, Impagliazzo A, Ubbink M (2004) A caged lanthanide complex as a paramagnetic shift agent for protein NMR. Chemistry 10(13):3252–3260

Schwieters CD, Kuszewski JJ, Tjandra N, Clore GM (2003) The Xplor-NIH NMR molecular structure determination package. J Magn Reson 160:65–73

Spiess HW (1978) Rotation of molecules and nuclear spin relaxation. In: Diehl P, Fluck E, Kosfeld R (eds) NMR basic principles and progress, vol. 15. Springer-Verlag, Berlin Heidelberg, New York

Suzuki M, Neutzner A, Tjandra N, Youle RJ (2005) Novel structure of the N terminus in yeast Fis1 correlates with a specialized function in mitochondrial fission. J Biol Chem 280(22):21444–21452

Teng Q, Iqbal M, Cross TA (1992) Determination of the ^{13}C chemical shift and ^{14}N electric field gradient tensor orientations with respect to the molecular frame in a polypeptide. J Am Chem Soc 114:5312–5321

Tjandra N, Feller SE, Pastor RW, Bax A (1995) Rotational diffusion anisotropy of human ubiquitin from ^{15}N NMR relaxation. J Am Chem Soc 117:12562–12566

Tjandra N, Wingfield P, Stahl S, Bax A (1996) Anisotropic rotational diffusion of perdeuterated HIV protease from ^{15}N NMR relaxation measurements at two magnetic. J Biomol NMR 8:273–284

Tjandra N, Bax A (1997) Direct measurement of distances and angles in biomolecules by NMR in a dilute liquid crystalline medium. Science 278:1111–1114

Tjandra N, Garrett DS, Gronenborn AM, Bax A, Clore GM (1997) Defining long range order in NMR structure determination from the dependence of heteronuclear relaxation times on rotational diffusion anisotropy. Nat Struct Biol 4(6):443–449

Tolman JR, Flanagan JM, Kennedy MA, Prestegard JH (1995) Nuclear magnetic dipole interactions in field-oriented proteins – information for structure determination in solution. Proc Natl Acad Sci USA 92(20):9279–9283

Woessner DE (1962) Nuclear spin relaxation in ellipsoids undergoing rotational brownian motion. J Chem Phys 36:647–654

Wöhnert J, Franz KJ, Nitz M, Imperiali B, Schwalbe H (2003) Protein alignment by a coexpressed lanthanide-binding tag for the measurement of residual dipolar couplings. J Am Chem Soc 125:13338–13339